Theoretical Study of the Dynamic Electron-Spin-Polarization via Doublet-Quartet Quantum-Mixed State and the Time-Resolved ESR Spectra of the Quartet High-Spin State

## Yoshio Teki* and Takafumi Matsumoto

Division of Molecular Material Science, Graduate School of Science,

Osaka City University

3-3-138 Sugimoto, Sumiyoshi-ku, Osaka 558-8585 (Japan)

E-mail: teki@sci.osaka-cu.ac.jp

Supplementary Information Data

The time-resolved ESR spectra and the details of the spectral simulations of **1**, **2** and the parent π-radical **3**, the details of the eigenfield/exact-diagonalization hybrid method, the detail derivation of the unitary transformation matrixes and dynamic electron polarization density matrixes by the perturbation approach, the results of the molecular orbital calculations, are presented as the supplementary information. The dependence of the time-resolved ESR spectra of the SC state at 10 ns on the electron transfer rate constant is also presented in this supplementary information.
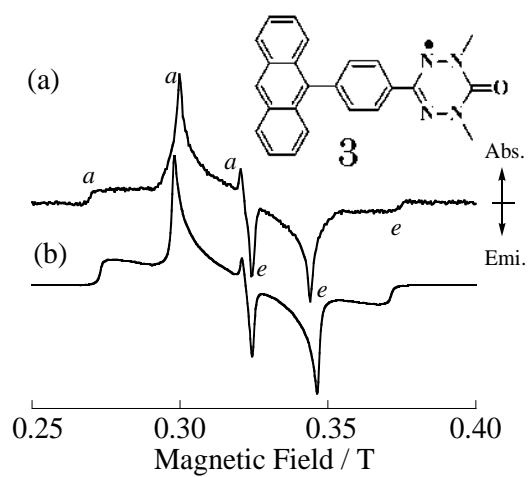
I) Time-Resolved ESR spectra and the details of the spectral simulations of 1, 2 and the parent π-radical 3.
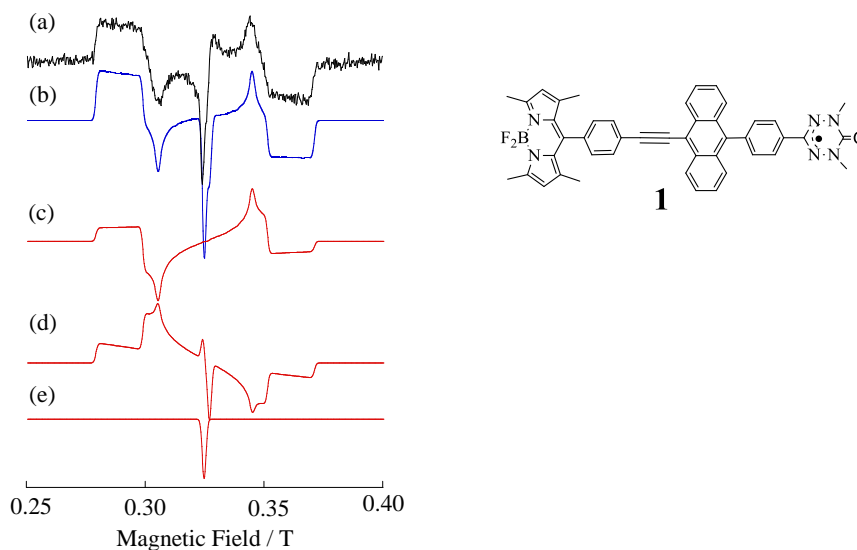
Figure S1 Observed time-resolved ESR spectrum of **1** and details of the spectral simulation.[29, 30] (a) Observed TRESR spectrum after laser excitation of the absorption band (λ = 505 nm) of the bodipy component **A**; (b) Simulation obtained by the superimposition of (c), (d) and (e) with the weight of 0.45, 0.55, and 0.14, respectively; (c) Simulation spectrum obtained by the selective population to the high-field spin-sublevels; (d) simulation spectrum obtained by the selective population to zero-field spin-sublevels (enhanced spin-orbit intersystem crossing mechanism); (e) simulation of polarized doublet state with $g = 2.005$.
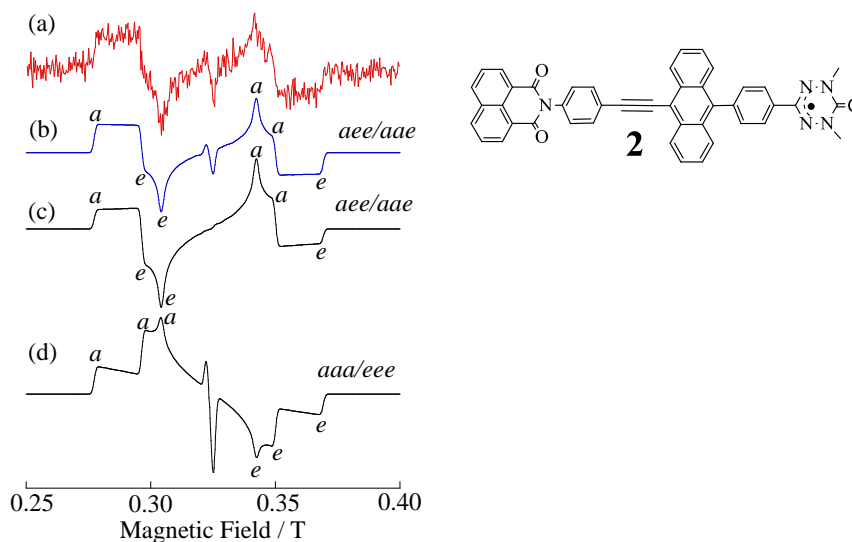
Figure S2 Observed time-resolved ESR spectrum of **2** and details of the spectral simulation (Y. Takemoto and Y. Teki, *ChemPhysChem*, published online. DOI:10.1002/cphc.201000709). (a) Observed TRESR spectrum obtained at 0.3 μs by the excitation of λ = 355 nm. (b) Simulation obtained by the superimposition of (c) and (d) with the weight of 0.78 : 0.22, respectively. (b) Simulation spectrum obtained by the selective population to the high-field spin-sublevels (novel mechanism through ion-pair state); (c) simulation spectrum obtained by the selective population to zero-field spin-sublevels (enhanced spin-orbit intersystem crossing mechanism).

2

Figure S3 Observed time-resolvedESR spectrum of the parent π-radical **3** and the spectral simulation.[13] (a) Time-resolved ESR at 30 K in 2-MTHF glass matrix. (b) Simulation. The simulation spectrum was obtained by the selective population to zero-field spin-sublevels (enhanced spin-orbit interystem crossing mechanism).

II) Details of the eigenfield/exact-diagonalization hybrid method

The eigenfield/exact-diagonalization hybrid method[48] is a combination of the eigenfield method[47] (exact calculation of the ESR resonance fields) and the numerical diagonalization of the spin-Hamiltonian. In this method, the resonance field $B_{Res}(\theta, \phi)$ for each transition of $Ms\leftrightarrow Ms'$ was directly calculated by solving the following eigenfield equation[47]:

$$A \bullet Z = B_{Res} C \bullet Z \quad , \tag{S1}$$

where A and C are given by the following super-operators.

$$A = \omega E \otimes E - F \otimes E + E \otimes F \tag{S2}$$

and

$$C = G \otimes E - E \otimes G^* \tag{S3}$$

Here, E is a unit matrix and ω is the given microwave frequency. The operators G and F are the field dependent and independent parts of the spin Hamiltonian, respectively. By solving the eigenfield equation (eq (S1)), the resonance fields (B_{Res}) are obtained. The transition probabilities $I(\theta, \phi, \varphi)$ were evaluated by numerically diagonalization of the spin Hamiltonian matrix at each calculated resonance eigenfield.

III) Details of the Perturbation Approach

We have treated the case of $|H_{ex}| < |H_f| << |H_z|$. Thus, $|H_f|$ and $|H_{ex}|$ were treated as perturbation terms. According to the conventional perturbation theory, the following equations have been derived. The energies (E_1 - E_6) and eigenfunctions ($|\phi_1>$ - $|\phi_6>$) are given by eqs. ($B1a$) – ($B1l$) in the Appendix of the main text. The unitary transformation matrix ($U^{W\to\phi}(\theta_1, \phi_1, \varphi_1, B)$) from the W basis representation to the ϕ basis representation is obtained to the first order using eqs. ($B1a$) – ($B1l$).

$$U^{W\to\phi}(\theta_1,\phi_1,\varphi_1,B) = \begin{pmatrix} 1 & -\dfrac{(D_1^{QM})^*}{\sqrt{2}\omega_T} & -\dfrac{(D_2^{QM})^*}{4\omega_T} & 0 & 0 & 0 \\[2ex] \dfrac{D_1^{QM}}{\sqrt{2}\omega_T} & 1 & \dfrac{(D_1^{QM})^*}{\sqrt{2}\omega_T} & -\dfrac{\sqrt{2}J_W}{\Delta_-} & 0 & 0 \\[2ex] \dfrac{D_2^{QM}}{4\omega_T} & -\dfrac{D_1^{QM}}{\sqrt{2}\omega_T} & 1 & 0 & -\dfrac{\sqrt{2}J_W}{\Delta_+} & 0 \\[2ex] 0 & \dfrac{\sqrt{2}J_W}{\Delta_-} & 0 & 1 & -\dfrac{(D_1^{QM})^*}{\sqrt{2}\omega_T} & -\dfrac{(D_2^{QM})^*}{4\omega_T} \\[2ex] 0 & 0 & \dfrac{\sqrt{2}J_W}{\Delta_+} & \dfrac{D_1^{QM}}{\sqrt{2}\omega_T} & 1 & \dfrac{(D_1^{QM})^*}{\sqrt{2}\omega_T} \\[2ex] 0 & 0 & 0 & \dfrac{D_2^{QM}}{4\omega_T} & -\dfrac{D_1^{QM}}{\sqrt{2}\omega_T} & 1 \end{pmatrix} \quad (S4)$$

Using this equation and the projection operator given in eq. ($A4$) in the Appendix of the main text, $\rho(t_1)_C^{QM}$ of eq.(5) is obtained to the first order on the ϕ basis representation as

$$\rho(t_1)_C^{QM} = U^{W\to\phi}(\theta_1,\phi_1,\varphi_1,B)^{-1}\hat{P}(D)U^{W\to\phi}(\theta_1,\phi_1,\varphi_1,B)$$

$$= \begin{pmatrix} 0 & \dfrac{(D_1^{QM})^*}{6\sqrt{2}\omega_T} & \dfrac{(D_2^{QM})^*}{12\omega_T} & -\dfrac{(D_1^{QM})^*}{6\omega_T} & -\dfrac{(D_2^{QM})^*}{12\sqrt{2}\omega_T} & 0 \\[2ex] \dfrac{D_1^{QM}}{6\sqrt{2}\omega_T} & \dfrac{1}{6}(1-\dfrac{4J_W}{\Delta_-}) & -\dfrac{(D_1^{QM})^*}{6\sqrt{2}\omega_T} & -\dfrac{\sqrt{2}}{6}(1-\dfrac{J_W}{\Delta_-}) & \dfrac{(D_1^{QM})^*}{3\omega_T} & \dfrac{(D_2^{QM})^*}{12\sqrt{2}\omega_T} \\[2ex] \dfrac{D_2^{QM}}{12\omega_T} & -\dfrac{D_1^{QM}}{6\sqrt{2}\omega_T} & \dfrac{1}{3}(1-\dfrac{2J_W}{\Delta_+}) & -\dfrac{D_1^{QM}}{3\omega_T} & -\dfrac{\sqrt{2}}{6}(1+\dfrac{J_W}{\Delta_+}) & -\dfrac{(D_1^{QM})^*}{6\omega_T} \\[2ex] -\dfrac{D_1^{QM}}{6\omega_T} & -\dfrac{\sqrt{2}}{6}(1-\dfrac{J_W}{\Delta_+}) & -\dfrac{(D_1^{QM})^*}{3\omega_T} & \dfrac{1}{3}(1+\dfrac{2J_W}{\Delta_-}) & -\dfrac{(D_1^{QM})^*}{6\sqrt{2}\omega_T} & -\dfrac{(D_2^{QM})^*}{12\omega_T} \\[2ex] -\dfrac{D_2^{QM}}{12\sqrt{2}\omega_T} & \dfrac{D_1^{QM}}{3\omega_T} & -\dfrac{\sqrt{2}}{6}(1+\dfrac{J_W}{\Delta_+}) & -\dfrac{D_1^{QM}}{6\sqrt{2}\omega_T} & \dfrac{1}{6}(1+\dfrac{4J_W}{\Delta_+}) & \dfrac{(D_1^{QM})^*}{6\sqrt{2}\omega_T} \\[2ex] 0 & \dfrac{D_2^{QM}}{12\sqrt{2}\omega_T} & -\dfrac{D_1^{QM}}{6\omega_T} & -\dfrac{D_2^{QM}}{12\omega_T} & \dfrac{D_1^{QM}}{6\sqrt{2}\omega_T} & 0 \end{pmatrix}_\phi \quad (S5)$$

This equation shows that the first order term D_0 ($\equiv -D_{zz}$) of the fine-structure tensor, $\boldsymbol{D}^{QM}$ is not contribute to the density matrix, which express the DEP of the QM state under the "finite field". Especially, it should be noted that the diagonal components of the density matrix (the populations of

the eigenstates of the QM state) is independent to the $\boldsymbol{D}^{QM}$. The de-coherence process leads to the density matrix $\rho(t_1)_{DC}^{QM}$, which is given by eq. (12) in the main text as follows.

$$
\rho(t_2)_{DC}^{QM} = \begin{pmatrix}
0 & 0 & 0 & 0 & 0 & 0 \\
0 & \dfrac{1}{6}(1-\dfrac{4J_W}{\Delta_-}) & 0 & 0 & 0 & 0 \\
0 & 0 & \dfrac{1}{3}(1-\dfrac{2J_W}{\Delta_+}) & 0 & 0 & 0 \\
0 & 0 & 0 & \dfrac{1}{3}(1+\dfrac{2J_W}{\Delta_-}) & 0 & 0 \\
0 & 0 & 0 & 0 & \dfrac{1}{6}(1+\dfrac{4J_W}{\Delta_+}) & 0 \\
0 & 0 & 0 & 0 & 0 & 0
\end{pmatrix}_{\phi}
\tag{12}
$$

Using eqs. (12), (A2) and (S4), the density matrix $\rho(t_3)_C^S$, on the high-field spin-eigenstates representation ($|Q_{3/2}\rangle$, $|Q_{1/2}\rangle$, $|Q_{-1/2}\rangle$, $|Q_{-3/2}\rangle$, $|D_{1/2}\rangle$, and $|D_{-1/2}\rangle$) is obtained to the first order as

$$
\rho(t_3)_C^S = (U^{W\to S})^{-1}(U^{\phi\to W})^{-1}\rho(t_2)_{DC}^{QM}U^{\phi\to W}U^{W\to S}
$$

$$
= \begin{pmatrix}
0 & -\dfrac{(D_1^{QM})^*}{6\sqrt{3}\omega_T} & -\dfrac{(D_2^{QM})^{\text{\textasciigrave}}}{12\sqrt{3}\omega_T} & 0 & \dfrac{(D_1^{QM})^*}{6\sqrt{6}\omega_T} & \dfrac{(D_2^{QM})^*}{6\sqrt{6}\omega_T} \\
-\dfrac{D_1^{QM}}{6\sqrt{3}\omega_T} & \dfrac{2}{9}(1-\dfrac{2J_W}{\Delta_-}) & \dfrac{(D_1^{QM})^*}{9\omega_T} & \dfrac{(D_2^{QM})^*}{12\sqrt{3}\omega_T} & \dfrac{\sqrt{2}}{18}(1+7J_W/\Delta_-) & -\dfrac{\sqrt{2}(D_1^{QM})^*}{36\omega_T} \\
-\dfrac{D_2^{QM}}{12\sqrt{3}\omega_T} & \dfrac{D_1^{QM}}{9\omega_T} & \dfrac{2}{9}(1+\dfrac{2J_W}{\Delta_+}) & -\dfrac{(D_1^{QM})^*}{6\sqrt{3}\omega_T} & \dfrac{\sqrt{2}D_1^{QM}}{36\omega_T} & -\dfrac{\sqrt{2}}{18}(1-\dfrac{7J_W}{\Delta_+}) \\
0 & \dfrac{D_2^{QM}}{12\sqrt{3}\omega_T} & -\dfrac{D_1^{QM}}{6\sqrt{3}\omega_T} & 0 & \dfrac{D_2^{QM}}{6\sqrt{6}\omega_T} & -\dfrac{D_1^{QM}}{6\sqrt{6}\omega_T} \\
\dfrac{D_1^{QM}}{6\sqrt{6}\omega_T} & \dfrac{\sqrt{2}}{18}(1+\dfrac{7J_W}{\Delta_-}) & \dfrac{\sqrt{2}D_1^{QM}}{36\omega_T} & \dfrac{(D_2^{QM})^*}{6\sqrt{6}\omega_T} & \dfrac{5}{18}(1+\dfrac{8J_W}{5\Delta_-}) & \dfrac{(D_1^{QM})^*}{9\omega_T} \\
\dfrac{D_2^{QM}}{6\sqrt{6}\omega_T} & -\dfrac{\sqrt{2}(D_1^{QM})^*}{36\omega_T} & -\dfrac{\sqrt{2}}{18}(1-\dfrac{7J_W}{\Delta_+}) & -\dfrac{(D_1^{QM})^*}{6\sqrt{6}\omega_T} & \dfrac{D_1^{QM}}{9\omega_T} & \dfrac{5}{18}(1-\dfrac{8J_W}{5\Delta_+})
\end{pmatrix}_S
\tag{S6}
$$

This equation shows that the DEP generated on the QM states is mainly transferred to the $M_S = \pm 1/2$ spin sublevels of the high-field wavefunctions of the SC states ($|Q_{\pm 1/2}\rangle$ and $|D_{\pm 1/2}\rangle$), which leads to a non-Boltzmann population (DEP). Thus, the M_S value is conserved during this process. The main off-diagonal terms are $\sqrt{2}(1+7J_W/\Delta_-)/18$ and $-\sqrt{2}(1-7J_W/\Delta_+)/18$. However, these terms do not contribute to the time-resolved ESR spectrum of the SC states as the "steady states" after the de-coherence.

In the SC states, the exchange interaction is much larger than other interactions. Here, we have treated the case of $|H_Z| > |H_f|$, and H_f as a perturbation term for H_Z. The mixing term V_{DQ} has been also incorporated as the perturbation for H_{ex}. According to the perturbation theory, the energies ($E(Q_{3/2})$ - $E(D_{-1/2})$) and the eigenfunctions ($|\Psi(Q_{3/2})\rangle$ - $|\Psi(D_{-1/2})\rangle$) are given by eqs. (B2a) − (B2l) in the Appendix of the main text. using eqs. (B1a) − (B1l). The unitary transformation matrix ($U^{\Psi\to S}(\theta_2, \phi_2, \varphi_2, B)$) from the Ψ basis to the S basis is obtained to the first

order using eqs. $(B1a) - (B1l)$:

$$U^{S \to \Psi}(\theta_2, \phi_2, \varphi_2, H) = \begin{pmatrix} 1 & -\dfrac{\sqrt{3}(D_1^Q)^*}{\omega_Q} & -\dfrac{\sqrt{3}(D_2^Q)^*}{4\omega_Q} & 0 & -\dfrac{(D_1^Q)^*}{\sqrt{6}J_S} & \dfrac{(D_2^Q)^*}{\sqrt{6}J_S} \\ \dfrac{\sqrt{3}D_1^Q}{\omega_Q} & 1 & 0 & -\dfrac{\sqrt{3}(D_2^Q)^*}{4\omega_Q} & \dfrac{\Omega_-}{3J_S} & \dfrac{(D_1^Q)^*}{\sqrt{2}J_S} \\ \dfrac{\sqrt{3}D_2^Q}{4\omega_Q} & 0 & 1 & \dfrac{\sqrt{3}(D_1^Q)^*}{\omega_Q} & \dfrac{D_1^Q}{\sqrt{2}J_S} & \dfrac{\Omega_+}{3J_S} \\ 0 & \dfrac{\sqrt{3}D_2^Q}{4\omega_Q} & -\dfrac{\sqrt{3}D_1^Q}{\omega_Q} & 1 & \dfrac{D_2^Q}{\sqrt{6}J_S} & -\dfrac{D_1^Q}{\sqrt{6}J_S} \\ \dfrac{D_1^Q}{\sqrt{6}J_S} & -\dfrac{\Omega_-}{3J_S} & -\dfrac{(D_1^Q)^*}{\sqrt{2}J_S} & -\dfrac{(D_2^Q)^*}{\sqrt{6}J_S} & 1 & 0 \\ \dfrac{D_2^Q}{\sqrt{6}J_S} & -\dfrac{D_1^Q}{\sqrt{2}J_S} & -\dfrac{\Omega_+}{3J_S} & \dfrac{(D_1^Q)^*}{\sqrt{6}J_S} & 0 & 1 \end{pmatrix} \quad (S7)$$

Using eqs. ($S6$) and ($S7$), $\rho(t_3)_C^\psi$ is obtained to the first order on the Ψ basis representation by

$$\rho(t_3)_C^\Psi = (U^{S \to \Psi})^{-1}\rho(t_3)_C^S U^{S \to \Psi}$$

$$= (U^{S \to \Psi})^{-1}(U^{W \to S})^{-1}(U^{\phi \to W})^{-1}\rho(t_2)_{DC}^{QM} U^{\phi \to W}U^{W \to S}U^{S \to \Psi} =$$

$$\begin{pmatrix} 0 & \begin{matrix} -\dfrac{(D_1^{QM})^*}{6\sqrt{3}\omega_T} \\ +\dfrac{(D_1^Q)^*}{18\sqrt{3}}(\dfrac{12}{\omega_Q}+\dfrac{1}{J_S}) \end{matrix} & \begin{matrix} -\dfrac{(D_2^{QM})^*}{12\sqrt{3}\omega_T} \\ +\dfrac{(D_2^Q)^*}{18\sqrt{3}}(\dfrac{3}{\omega_Q}-\dfrac{1}{J_S}) \end{matrix} & 0 & \begin{matrix} \dfrac{(D_1^{QM})^*}{6\sqrt{6}\omega_T} \\ +\dfrac{(D_1^Q)^*}{18\sqrt{3}}(\dfrac{6}{\omega_Q}+\dfrac{5}{J_S}) \end{matrix} & \begin{matrix} \dfrac{(D_2^{QM})^*}{6\sqrt{6}\omega_T} \\ -\dfrac{(D_2^Q)^*}{36\sqrt{6}}(\dfrac{3}{\omega_Q}-\dfrac{10}{J_S}) \end{matrix} \\[2em] \begin{matrix} -\dfrac{D_1^{QM}}{6\sqrt{3}\omega_T} \\ +\dfrac{D_1^Q}{18\sqrt{3}}(\dfrac{12}{\omega_Q}+\dfrac{1}{J_S}) \end{matrix} & \begin{matrix} \dfrac{2}{9}(1-\dfrac{2J_W}{\Delta_-}) \\ -\dfrac{\sqrt{2}\Omega_-}{27J_S} \end{matrix} & \dfrac{(D_1^{QM})^*}{9\omega_T} & \begin{matrix} \dfrac{(D_2^{QM})^*}{12\sqrt{3}\omega_T} \\ -\dfrac{(D_2^Q)^*}{18\sqrt{3}}(\dfrac{3}{\omega_Q}+\dfrac{1}{J_S}) \end{matrix} & \begin{matrix} \dfrac{\sqrt{2}}{18}(1+\dfrac{7J_W}{\Delta_-}) \\ -\dfrac{\Omega_-}{54J_S} \end{matrix} & \begin{matrix} -\dfrac{\sqrt{2}(D_1^{QM})^*}{36\omega_T} \\ -\dfrac{\sqrt{2}(D_1^Q)^*}{36J_S} \end{matrix} \\[2em] \begin{matrix} -\dfrac{D_2^{QM}}{12\sqrt{3}\omega_T} \\ +\dfrac{D_2^Q}{18\sqrt{3}}(\dfrac{3}{\omega_Q}-\dfrac{1}{J_S}) \end{matrix} & \dfrac{D_1^{QM}}{9\omega_T} & \begin{matrix} \dfrac{2}{9}(1+\dfrac{2J_W}{\Delta_+}) \\ +\dfrac{\sqrt{2}\Omega_+}{27J_S} \end{matrix} & \begin{matrix} -\dfrac{(D_1^{QM})^*}{6\sqrt{3}\omega_T} \\ +\dfrac{(D_1^Q)^*}{18\sqrt{3}}(\dfrac{12}{\omega_Q}-\dfrac{1}{J_S}) \end{matrix} & \begin{matrix} \dfrac{\sqrt{2}D_1^{QM}}{36\omega_T} \\ -\dfrac{\sqrt{2}D_1^Q}{36J_S} \end{matrix} & \begin{matrix} -\dfrac{\sqrt{2}}{18}(1-\dfrac{7J_W}{\Delta_+}) \\ -\dfrac{\Omega_+}{54J_S} \end{matrix} \\[2em] 0 & \begin{matrix} \dfrac{D_2^{QM}}{12\sqrt{3}\omega_T} \\ -\dfrac{D_2^Q}{18\sqrt{3}}(\dfrac{3}{\omega_Q}+\dfrac{1}{J_S}) \end{matrix} & \begin{matrix} -\dfrac{D_1^{QM}}{6\sqrt{3}\omega_T} \\ +\dfrac{D_1^Q}{18\sqrt{3}}(\dfrac{12}{\omega_Q}-\dfrac{1}{J_S}) \end{matrix} & 0 & \begin{matrix} \dfrac{D_2^{QM}}{6\sqrt{6}\omega_T} \\ -\dfrac{D_2^Q}{36\sqrt{6}}(\dfrac{3}{\omega_Q}+\dfrac{10}{J_S}) \end{matrix} & \begin{matrix} -\dfrac{D_1^{QM}}{6\sqrt{6}\omega_T} \\ -\dfrac{D_1^Q}{18\sqrt{6}}(\dfrac{6}{\omega_Q}-\dfrac{5}{J_S}) \end{matrix} \\[2em] \begin{matrix} \dfrac{D_1^{QM}}{6\sqrt{6}\omega_T} \\ +\dfrac{D_1^Q}{18\sqrt{6}}(\dfrac{6}{\omega_Q}+\dfrac{5}{J_S}) \end{matrix} & \begin{matrix} \dfrac{\sqrt{2}}{18}(1+\dfrac{J_W}{\Delta_-}) \\ -\dfrac{\Omega_-}{54J_S} \end{matrix} & \begin{matrix} \dfrac{\sqrt{2}(D_1^{QM})^*}{36\omega_T} \\ -\dfrac{\sqrt{2}(D_1^Q)^*}{36J_S} \end{matrix} & \begin{matrix} \dfrac{(D_2^{QM})^*}{6\sqrt{6}\omega_T} \\ -\dfrac{(D_2^Q)^*}{36\sqrt{6}}(\dfrac{3}{\omega_Q}+\dfrac{10}{J_S}) \end{matrix} & \begin{matrix} \dfrac{5}{18}(1+\dfrac{8J_W}{5\Delta_-}) \\ +\dfrac{\sqrt{2}\Omega_-}{27J_S} \end{matrix} & \dfrac{(D_1^{QM})^*}{9\omega_T} \\[2em] \begin{matrix} \dfrac{D_2^{QM}}{6\sqrt{6}\omega_T} \\ -\dfrac{D_2^Q}{36\sqrt{6}}(\dfrac{3}{\omega_Q}-\dfrac{10}{J_S}) \end{matrix} & \begin{matrix} -\dfrac{\sqrt{2}D_1^{QM}}{36\omega_T} \\ -\dfrac{\sqrt{2}D_1^Q}{36J_S} \end{matrix} & \begin{matrix} -\dfrac{\sqrt{2}}{18}(1-\dfrac{7J_W}{\Delta_+}) \\ -\dfrac{\Omega_+}{54J_S} \end{matrix} & \begin{matrix} -\dfrac{(D_1^{QM})^*}{6\sqrt{6}\omega_T} \\ -\dfrac{(D_1^Q)^*}{18\sqrt{6}}(\dfrac{6}{\omega_Q}-\dfrac{5}{J_S}) \end{matrix} & \dfrac{D_1^{QM}}{9\omega_T} & \begin{matrix} \dfrac{5}{18}(1-\dfrac{8J_W}{5\Delta_+}) \\ -\dfrac{\sqrt{2}\Omega_+}{27J_S} \end{matrix} \end{pmatrix}_\Psi \quad (S8)$$

The de-coherence process during $t_3 - t_4$ leads to the selectively populated SC spin eigenstates which is represented by eq. (15) on the Ψ basis representation shown in the main text as follows.

$$\rho(t_4)_{DC}^{\Psi} = \begin{pmatrix} 0 & 0 & 0 & 0 & 0 & 0 \\ 0 & \dfrac{2}{9}(1-\dfrac{2J_W}{\Delta_-})-\dfrac{\sqrt{2}\Omega_-}{27J_S} & 0 & 0 & 0 & 0 \\ 0 & 0 & \dfrac{2}{9}(1+\dfrac{2J_W}{\Delta_+})+\dfrac{\sqrt{2}\Omega_+}{27J_S} & 0 & 0 & 0 \\ 0 & 0 & 0 & 0 & 0 & 0 \\ 0 & 0 & 0 & 0 & \dfrac{5}{18}(1+\dfrac{8J_W}{5\Delta_-})+\dfrac{\sqrt{2}\Omega_-}{27J_S} & 0 \\ 0 & 0 & 0 & 0 & 0 & \dfrac{5}{18}(1-\dfrac{8J_W}{5\Delta_+})-\dfrac{\sqrt{2}\Omega_+}{27J_S} \end{pmatrix}_{\Psi} \tag{15}$$

IV) Results of the *ab-initio* molecular orbital calculations

(a)
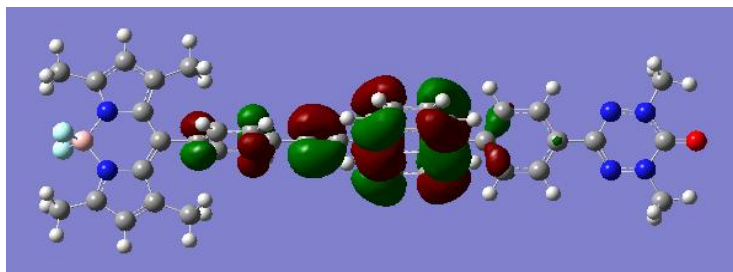
(b)
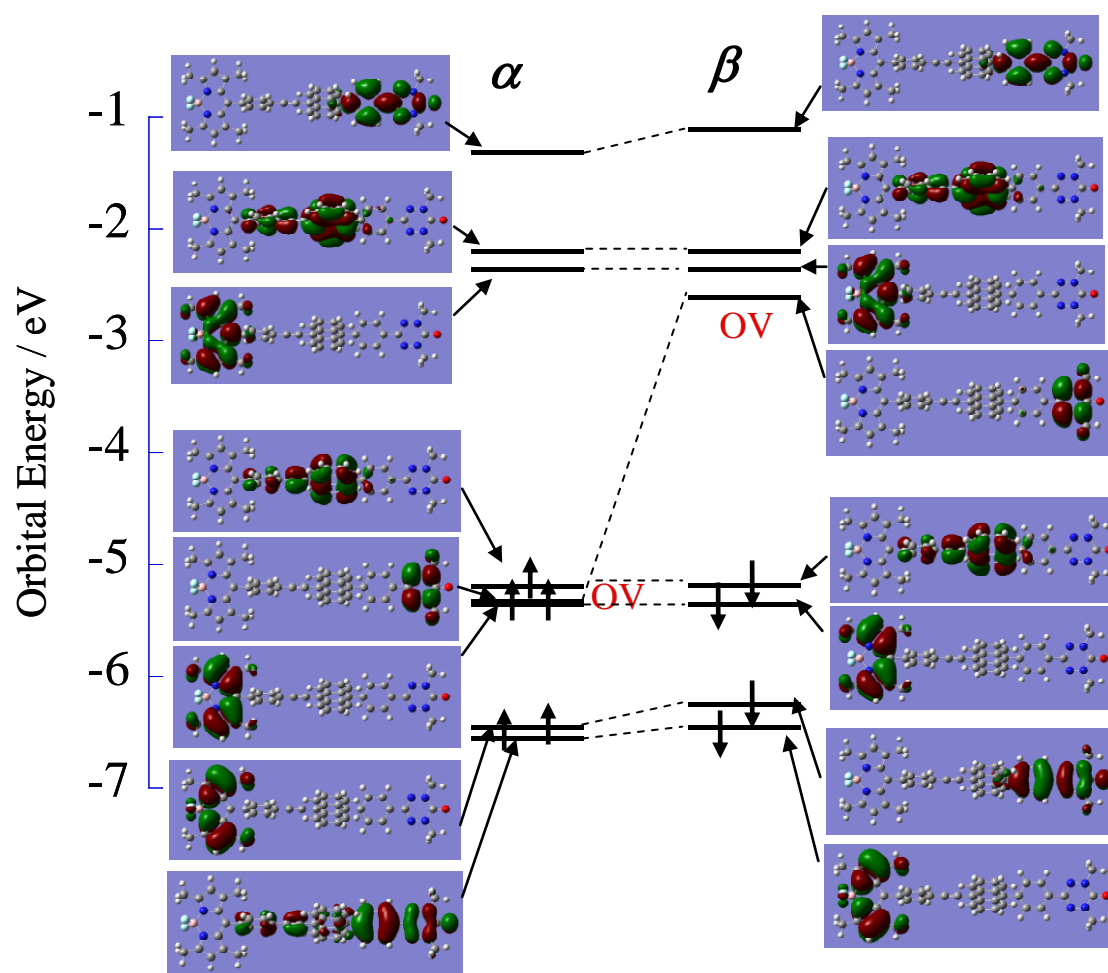
Total Energy: *E* = -2364.93328927 a.u.

Figure S4 (a) π-HOMO and (b) MO level diagram of the ground state of **1**

(a)
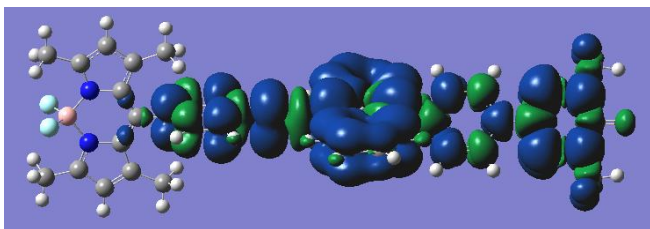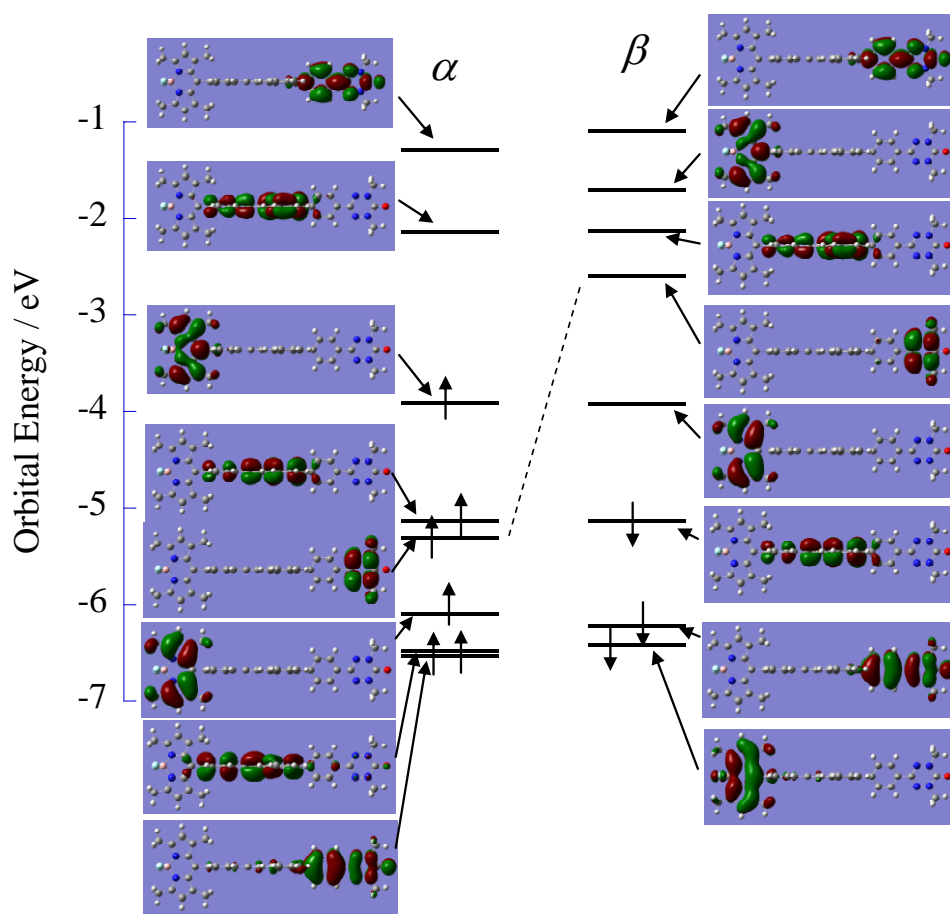

(b)

MO Diagram of BODIPY-An-OV (Quartet Excited State)

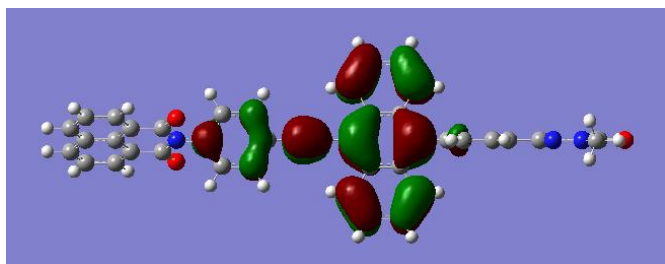α β

Orbital Energy / eV

-1

-2

-3

-4

-5

-6

OV

OV
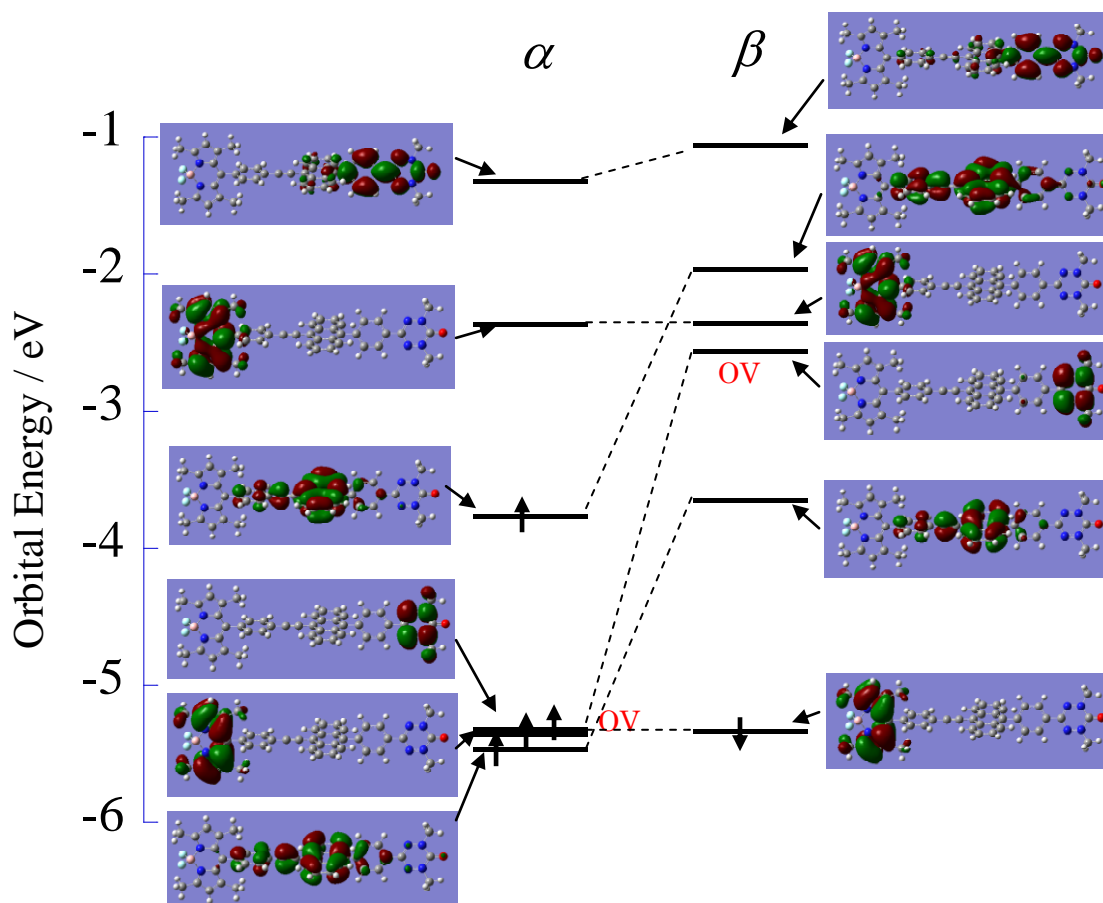
Total Energy: $E = -2364.88064$ a.u.

Figure S5 (a) Spin density distribution and (b) molecular orbitals and energy levels of the quartet photo-excited state of **1**.

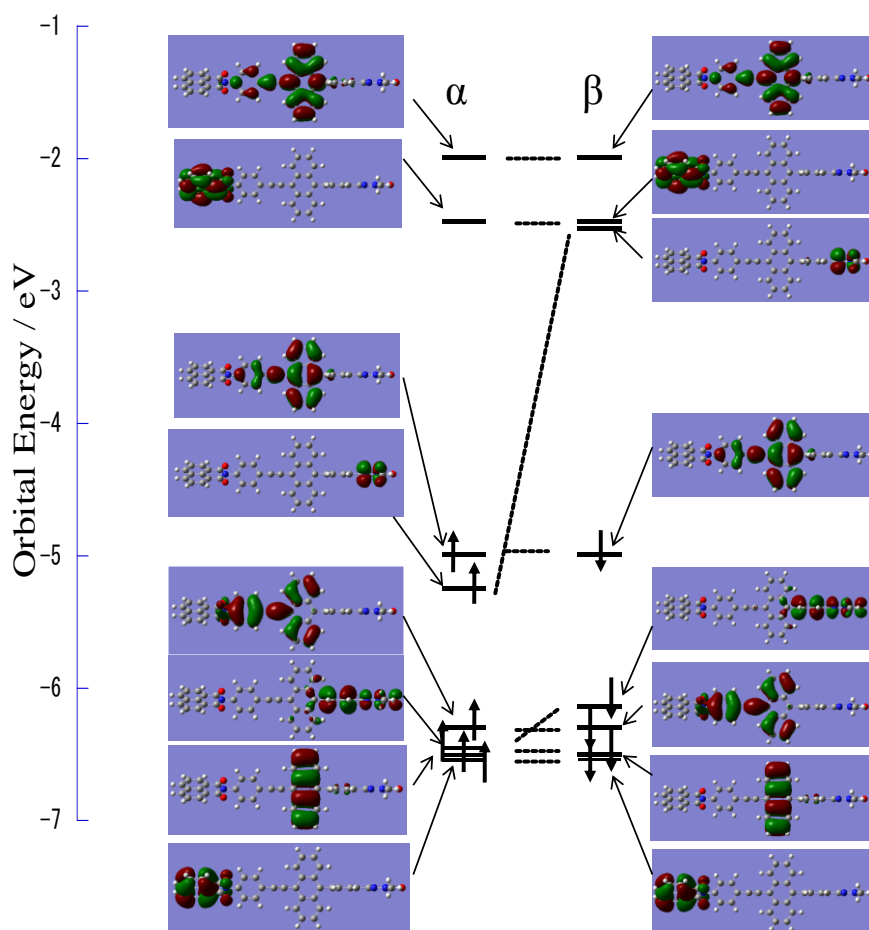(a)
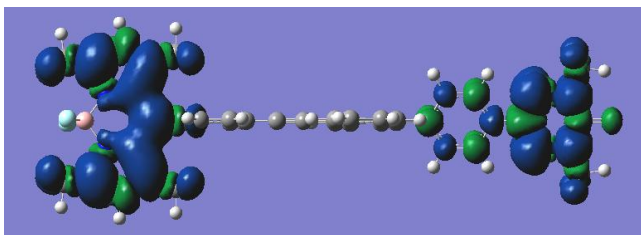
(b)

Total Energy: E(UB3LYP) = - 2364.87771 a.u.

Figure S6 (a) Spin density distribution and (b) molecular orbitals and energy levels of the another photo-excited QM state of **1**, which is constructed from the photo-excited triplet state of the BODIPY moiety and the spin-doublet radical moiety. This photo-excited state is higher in energy about 0.0029_3 a.u. (0.079 eV) than the quartet state detected by time-resolved ESR.
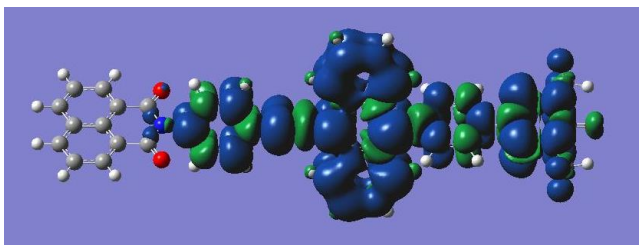
(a)

(b)

MO Diagram of Naphtalimide-An-Ver (Ground State)
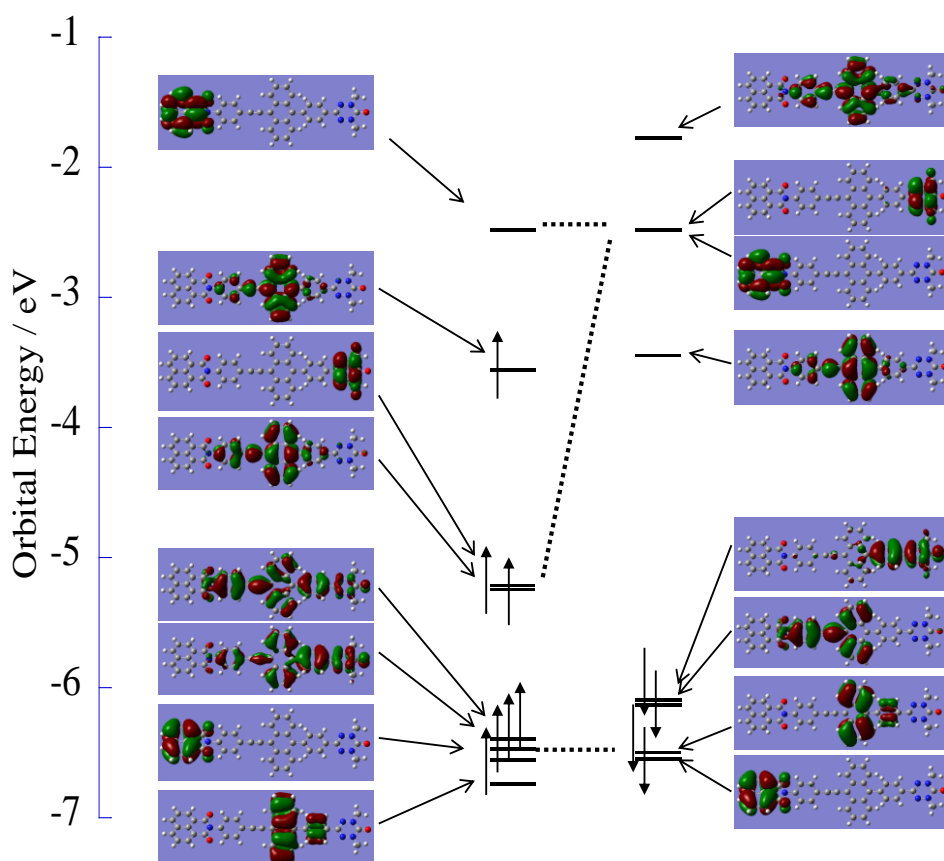

Total Energy: E(UB3LYP) = -2193.00289 a.u.

Figure S7 (a) π-HOMO and (b) MO level diagram of the ground state of **2**[41]

(a)

(b)

MO Diagram of Naphtalimide-An-Ver (Quartet State)


Total Energy: E(UB3LYP) = -2192.94981 a.u.

Figure S8 (a) Spin density distribution and (b) molecular orbitals and energy levels of the quartet photo-excited state of **2**.[41]

V) Dependence of the time-resolved ESR spectra of the SC state at 10 ns on the electron transfer rate constant

Using the solution (26), $I^{QM} = I^{SC} = 0$ and the initial condition ($\rho(0)^{QM} = P(D)$ and $\rho(0)^{SC} = 0$ on the W basis representation), we simulated the dependence of the time-resolved ESR spectra of the SC state on k_{ET}. Figure S10 shows the dependence of the time-resolved ESR spectra of the SC state on the electron transfer rate constant. In this calculation the duration time was set to be 10 ns. As shown in this Figure, the most similar one to those obtained by the polarization transfer after the de-coherence of the QM state shown in Figures 13(a)-(f) is Figure (j). However, the center region of the spectrum is different from those shown in Figures 13(a)-(f). Thus, only the incomplete dephasing was obtained at 10 ns.
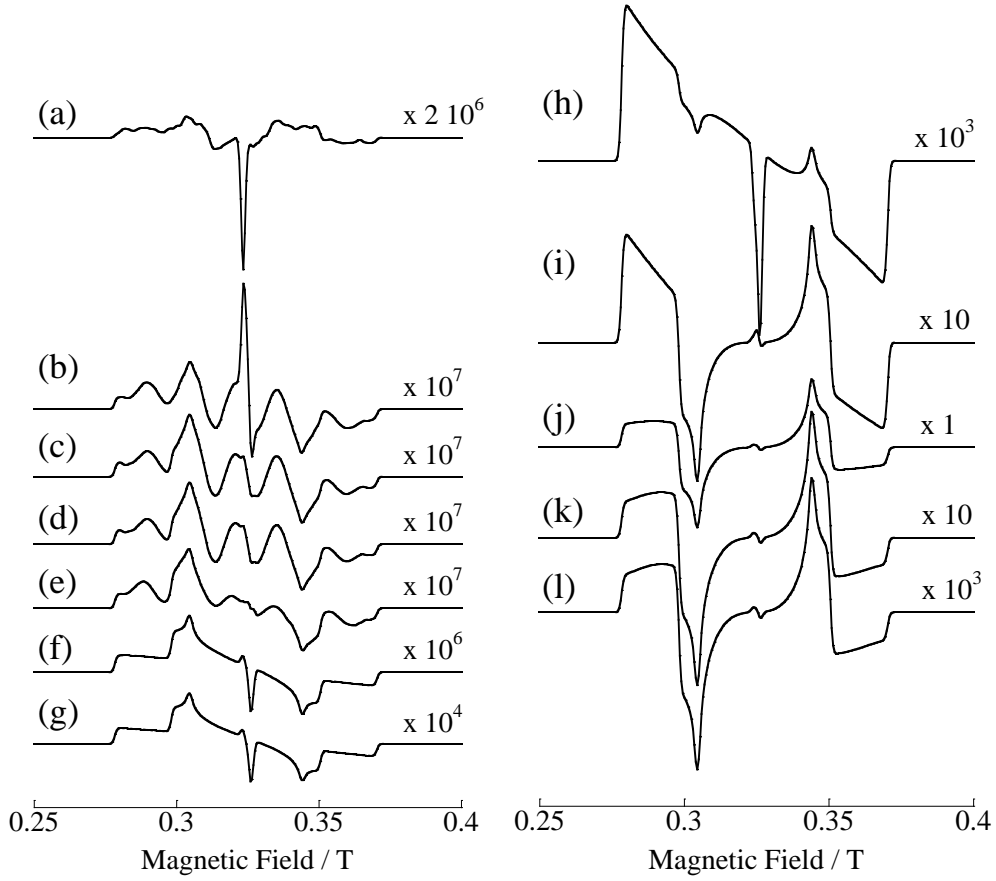
Figure S9 Dependence of the simulation spectra of the SC state on k_{ET}. The duration time was set to be 10 ns. $D^{SC} = 0.0645$ cm^{-1} and $E^{SC} = 0.0030$ cm^{-1} were used for the fine-structure parameter of the SC state. D^{QM}, $2J_W$ and $2J_S$ values were fixed to be 0.022 cm^{-1}, 0.05 MHz and 5000 GHz, respectively. (a) $k_{ET} = 1.0 \times 10^{17}$ s^{-1}, (b) $k_{ET} = 1.0 \times 10^{16}$ s^{-1}, (c) $k_{ET} = 1.0 \times 10^{15}$ s^{-1}, (d) $k_{ET} = 1.0 \times 10^{14}$ s^{-1} (e) $k_{ET} = 1.0 \times 10^{13}$ s^{-1}, (f) $k_{ET} = 1.0 \times 10^{12}$ s^{-1}, (g) $k_{ET} = 1.0 \times 10^{11}$ s^{-1}, (h) $k_{ET} = 1.0 \times 10^{10}$ s^{-1}, (i) $k_{ET} = 1.0 \times 10^{9}$ s^{-1} and (j) $k_{ET} = 1.0 \times 10^{8}$ s^{-1}, (k) $k_{ET} = 1.0 \times 10^{7}$ s^{-1} and (l) $k_{ET} = 1.0 \times 10^{6}$ s^{-1} respectively.